HHS Public Access

Author manuscript

Int J Imaging Syst Technol. Author manuscript; available in PMC 2017 June 01.

Published in final edited form as:

Int J Imaging Syst Technol. 2016 June ; 26(2): 106–115. doi:10.1002/ima.22165.

An Actively Decoupled Dual Transceiver Coil System for Continuous ASL at 7 T

Randall B. Stafford[1,2,3,*], **Myung-Kyun Woo**[4,5,6,*], **Se-Hong Oh**[1,2,7], **Sudipto Dolui**[1,2,8], **Tiejun Zhao**[9], **Young-Bo Kim**[4], **John A. Detre**[1,2,8], **Zang-Hee Cho**[4,10], and **Jongho Lee**[1,2,5]

[1]Department of Radiology, University of Pennsylvania, Philadelphia, PA, USA

[2]Center for Functional Neuroimaging, University of Pennsylvania, Philadelphia, PA, USA

[3]Department of Clinical Neurosciences, University of Calgary, Calgary, AB, Canada

[4]Neuroscience Research Institute, Gachon University, Incheon, Korea

[5]Department of Electrical and Computer Engineering, Seoul National University, Seoul, Korea

[6]Department of Electrical Engineering, University of Minnesota, Minneapolis, MN, USA

[7]Imaging Institute, Cleveland Clinic, Cleveland, OH, USA

[8]Department of Neurology, University of Pennsylvania, Philadelphia, PA, USA

[9]Siemens Medical Solutions USA, Inc., Siemens Healthcare, New York, NY, USA

[10]Advanced Institutes of Convergence Technology, Seoul National University, Seoul, Korea

Abstract

7 T arterial spin labeling (ASL) faces major challenges including the increased specific absorption rate (SAR) and increased B_0 and B_1 inhomogeneity. This work describes the design and implementation of a dual-coil system that allows for continuous ASL (CASL) at 7 T. This system consisted of an actively detunable eight-channel transceiver head coil, and a three-channel transceiver labeling coil. Four experiments were performed in 5 healthy subjects: (i) to demonstrate that active detuning during ASL labeling reduces magnetization transfer; (ii) to measure the B_1 profile at the labeling plane; (iii) to quantify B_0 off-resonance at the labeling plane; and (iv) to collect *in vivo* CASL data. The magnetization transfer ratio in the head coil was reduced to 0.0 ± 0.2% by active detuning during labeling. The measured B_1 profiles in all 5 subjects were sufficient to satisfy the flow-driven adiabatic inversion necessary for CASL, however the actual labeling efficiency was significantly impacted by B_0 off-resonance at the labeling plane. The measured CASL percent signal change in gray matter (0.94% ± 0.10%) corresponds with the low labeling efficiency predicted by the B_0 off-resonance. This work demonstrates progress in the technical implementation of 7 T CASL, and reinforces the need for improved B_0 homogeneity at the labeling plane.

Corresponding Authors: Jongho Lee, PhD, Department of Electrical and Computer Engineering, Seoul National University, Building 301, Room 1008, 1 Gwanak-ro, Gwanak-gu, Seoul, Korea, +82-2-880-7310, jonghoyi@snu.ac.kr. Zang-Hee Cho, PhD, Advanced Institutes of Convergence Technology, Seoul National University, 145 Gwangkyo-ro, Youngtong-gu, Suwon, Korea, zcho1@snu.ac.kr.

*These authors have equally contributed to this work

Keywords

magnetic resonance imaging; arterial spin labeling; 7 T; specific absorption rate; labeling coils; B_1-mapping; B_0-mapping

Introduction

Arterial spin labeling (ASL) has been used for non-invasive perfusion measurements with magnetic resonance imaging (MRI) for over two decades (Detre et al., 1992, Williams et al., 1992, Brown et al., 2007). The two main categories of ASL are (i) continuous or pseudo-continuous ASL (CASL and pCASL, respectively) (Detre et al., 1992, Williams et al., 1992, Maccotta et al., 1997, Alsop and Detre 1996, Detre and Alsop 1999, Dai et al., 2008, Jung et al., 2010, Wu et al., 2007), (ii) and pulsed ASL (PASL) (Edelman et al., 1994, Kim 1995, Kwong et al., 1995, Schwarzbauer et al., 1996, Wong et al., 1998). The underlying principles of these two techniques are the same: (1) a nominally diffusible endogenous tracer is generated by magnetically labeling in-flowing protons in arterial blood, and (2) the labeled blood flows into the tissue of interest. The resulting MR signal difference between an image collected with this magnetic labeling and a control image, collected in the absence of labeling, is directly proportional to the perfusion, and ultimately tissue function.

Magnetic labeling in ASL is typically achieved by inverting the equilibrium magnetization of arterial blood, either by applying large-slab 180° inversion pulses in PASL (Edelman et al., 1994, Kim 1995, Kwong et al., 1995, Schwarzbauer et al., 1996, Wong et al., 1998, Jahng et al., 2003), or via flow-driven adiabatic inversion in CASL (Dixon et al., 1986, Detre and Alsop 1999, Wu et al., 2007). Continuous flow-driven adiabatic inversion is generated in pCASL using a series of phase-corrected excitations. The half-life of the ASL tracer is proportional to the T_1 recovery rate of arterial blood magnetization. As demonstrated in animal models by Franke *et al.* (Franke et al., 2000) and Lu *et al.* (Lu et al., 2010), higher magnetic field will improve the overall quality of ASL perfusion measurements owing to the increased T_1 relaxation time (Dobre et al., 2007, Edelstein et al., 1986, Vaughan et al., 2001, Gonen et al., 2001), and increased MR signal (Gonen et al., 2001, Edelstein et al., 1986, Vaughan et al., 2001). The T_1 of arterial blood increases from roughly 1600 ms at 3 T to nearly 2100 ms at 7 T (Dobre et al., 2007). These complementary benefits suggest that the ASL signal increases supralinearly with increasing magnetic field strength (Franke et al., 2000). Expanding upon simulations by Wang *et al.* (Wang et al., 2002), assuming arterial blood T_1 of 2068 ms (Dobre et al., 2007), a tissue T_{2*} of 28 ms at 7 T (Govindarajan et al., 2015), and an expected CBF of 55 mL/100 g/min (Chen et al., 2011), the expected percent signal difference for CASL and pCASL increases from 1.4% at 3 T to 2.4% at 7 T, for the 85% labeling efficiency expected in CASL (Figure 1a). The increased ASL signal at 7 T potentially allows for reduced partial volume confounds such as white matter contamination (Hall et al., 2009), or more accurately measuring blood flow in weakly perfused tissues, such as skeletal muscle at rest (Raitakari et al., 1996) and cerebral white matter (van Gelderen et al., 2008, Gardener and Jezzard 2015). With the increased availability of 7 T human systems, ASL may ultimately prove to be an ideal application to benefit from ultra-high field

(UHF). However, there are many challenges that must be addressed before these benefits can be realized.

Preliminary work on *in vivo* CASL at 7 T showed promise of the expected benefits of ASL at UHF (Talagala et al., 2008, Wang et al., 2008), however the temporal signal-to-noise ratio (tSNR) measured at 7 T did not compare favorably with data from 3 T. Similarly, work by Gardener *et al.* (Gardener et al., 2009), which involved PASL labeling schemes, highlighted the limitations of both B_0 and B_1 inhomogeneity, and their negative impact on labeling efficiency. Recently, Gardener *et al.* (Gardener and Jezzard 2015) have had success using 7 T PASL for WM perfusion. Ghariq *et al.* (Ghariq et al., 2012) and Luh *et al.* (Luh et al., 2013) have reported *in vivo* results using pCASL at 7 T. These studies illustrate the sensitivity of pCASL to off-resonance at the labeling plane and the limitations of increased specific absorption rate (SAR) at higher fields. Another recent 7 T study by Wang *et al.* focused on combining pCASL with a turbo Fast Low Angle Shot (FLASH) (Frahm et al., 1986) readout (Zuo et al., 2013, Wang et al., 2015), along with accelerated simultaneous multi-slice acquisition strategies (Wang et al., 2015). While this readout technique shows promise for reducing image distortion and allowing for more consistent post-label delay times across the whole brain, the pCASL labeling duration is still subject to the same SAR limitations mentioned above.

The first major hurdle for ASL at 7 T is SAR deposition, which increases with the square of B_0 (Collins and Smith 2001). This SAR restriction is particularly challenging given that the optimal inversion bolus length also increases at higher field strengths (Lu et al., 2010). One consequence of higher SAR is an increase in the minimum allowed repetition time (TR) (Teeuwisse et al., 2010). However, despite the higher SAR burden with continuous ASL methods (Wang et al., 2002), CASL approaches would be preferred over PASL techniques for realizing the benefits of UHF (Teeuwisse et al., 2010) as CASL techniques can create an arbitrarily long bolus (SAR notwithstanding) that is not limited by the physical coverage of the radiofrequency (RF) coil (Teeuwisse et al., 2010).

Standard CASL has the advantage of lower SAR than pCASL owing to a lower peak B_1 power (Ghariq et al., 2012, Dai et al., 2008), despite the gaps between RF pulses in the pCASL labeling train (Luh et al., 2013). Previously, amplitude modulation of the control scheme has been introduced to mitigate magnetization transfer (MT) effects, thereby allowing for full-brain coverage with multi-slice CASL at the expense of reducing the overall labeling efficiency (Alsop and Detre 1998, Wang et al., 2005). The use of a separate labeling coil system allows for active decoupling of the head coil during RF transmission with the labeling coil (Talagala et al., 2004). Detuning of the head coil can eliminate MT effects in the brain during labeling, thereby removing the need for any MT matching (via RF transmission) during the unlabeled control scans (Teeuwisse et al., 2010). In addition to providing a 50% reduction in total SAR as compared to labeling schemes with an active control scan, excluding the control RF also allows for multi-slice CASL with equal labeling efficiency as pCASL (Alsop and Detre 1998).

A second obstacle that must be overcome before ASL can be realized at 7 T is the optimization of labeling efficiency, which is impacted by both B_0 (Luh et al., 2013, Wong

2007) and B_1 inhomogeneity (Teeuwisse et al., 2010). Figure 1b demonstrates the negative impact of B_0 off-resonance on labeling efficiency by expanding upon simulations by Maccotta *et al.* (Maccotta et al., 1997). Even in the absence of B_0 inhomogeneity, labeling efficiency is heavily dependent on the quality of the B_1 profile at the labeling plane (Teeuwisse et al., 2010). Given the sub-optimal B_1 profile of many 7 T head coils at the level of the extracranial carotid and vertebral arteries (Teeuwisse et al., 2010), one way to improve the B_1 at the labeling plane is to employ a separate labeling RF coil (Dixon et al., 1986, Silva et al., 1995, Talagala et al., 2004, Zaharchuk et al., 1999, Trampel et al., 2002, Wang et al., 2008, Hetzer et al., 2009). Unlike the 3 T labeling coil designed by Hetzer *et al.* (Hetzer et al., 2009), many of these previous implementations of external labeling coils did not include receive capabilities (Dixon et al., 1986, Silva et al., 1995, Talagala et al., 2004, Zaharchuk et al., 1999, Trampel et al., 2002), and rather rely on signal detection with the vendor-supplied body coil, or nearby pick-up coils. Because many 7 T systems lack a body coil, the use of transmit-only labeling coils could preclude an accurate measurement of the actual B_1 at the labeling plane due to a lack of optimal receive sensitivity of the head coil.

The research presented here describes the design and implementation of dual-coil hardware to allow CASL at 7 T. The system includes a detunable 8-channel transmit/receive (Tx/Rx) head coil to allow for control schemes that do not require MT matching via RF deposition with CASL, combined with a 3-channel transceiver labeling coil that also allows for accurate measurement of the B_1 profile at the labeling plane. The goal of this study was to develop and assess the utility of dual-coil system for CASL at 7 T.

Materials and Methods

System Design

Several combinations of labeling coils were tested prior to selection of the final design. These iterations included variations using two and three-channel labeling coils (a subset of these experiments have been presented previously (Stafford et al., 2012), but is excluded from the present work for brevity). During this initial design phase, our results suggested that two-coil variants placed near the carotids lacked sufficient B_1 penetration to reach the vertebral arteries, thus necessitating a third posterior coil (Stafford et al., 2012). Similarly, smaller labeling coil elements were found to produce inhomogeneous fields at the depths required for labeling of the carotid and/or the vertebral arteries, thus prompting the use of surface coils with slightly larger area (Woo et al., 2012).

The final coil design consisted of two separate transceiver coil arrays: (i) an actively detunable eight-channel head coil, and a three-channel labeling coil. The head coil channel elements were designed with an etched-pattern printed circuit board and constructed on an elliptical acrylic case (21 cm and 26 cm for the x-axis and y-axis, respectively). The eight-channel head coil was mounted on the rails of an acrylic half-pipe track, allowing the coil position to be adjusted in the superior-inferior direction. Each of the eight rectangular coils (10 cm wide × 20 cm long) was mounted on the acrylic case with a 45° phase shift relative to its nearest neighbors. The three channel elements of the labeling coil were printed with a square shape (10 cm × 10 cm), and mounted on ergonomic curved surfaces: acrylic for the posterior coil mounted under the original half-pipe track, and Lexan (SABIC Innovative

Plastics, Riyadh, Saudi Arabia) for the remaining coils, which were mounted on an MR-compatible neck brace (Stifneck by Laerdal Medical, Wappingers Falls, NY). The phase separation for the three labeling coils was 120°.

The lumped-element equivalent circuit diagram of the head coil with the active detuning circuit is shown in Fig. 2. The eight head coil elements were integrated with seven capacitors for tuning and three capacitors for matching. The capacitance for each of the tuning and matching components is indicated in Fig. 2. Each coil element was isolated by a capacitive decoupling circuit; the corresponding S_{12} value between adjacent coils was kept under −15 dB. The three labeling coil elements were tuned with three capacitors (2.7 pF-3.0 pF) and a matching network. The distance between each of the labeling coils was sufficiently large that additional decoupling was not needed. Each head and labeling coil was tuned to 297.2 MHz with standard human loading.

A TTL pulse was generated by the pulse sequence to control routing of RF power to either the labeling or head coils via an external RF switch. The same RF switch was used to control the PIN diodes used for the direct current bias detuning circuitry in the head coil. A network analyzer (Agilent 4395A, Agilent Technologies, Santa Clara, CA) was used for recording the detuning while the head coil was loaded with a human head. The detuned level of the head coil was regulated under −34dB as determined by a pickup probe

A custom interface controller box included 8-channel and 3-channel transmit/receive controllers for head imaging and labeling, respectively. The TTL switch was responsible for routing the power from the vendor-supplied RF amplifier to either the head or labeling coils. The transmit power was equally divided by a 2-way divider which routed power to two separate 4-way dividers for the 8-channel transmit/receive controller. The 3-channel transmit/receive controller consisted of a simple 3-way divider. Divided power was then transmitted to each channel of the head and labeling coils via transmit/receive switch circuits, respectively.

A computational electromagnetic simulation was performed using a commercial finite difference time domain (xFDTD; REMCOM, State College, PA) for simulating the expected RF transmit (B_{1+}) in the 3-channel labeling coil. The simulated position of the labeling coil with the head mesh model in xFDTD is shown in Fig. 3. All the geometries were modeled using the high-fidelity head model, which includes the shoulders with $2 \times 2 \times 2$ mm^3 resolution. Each channel of the labeling coil was driven by 3 sources with identical amplitude and a 120° phase shift between channels. The 120° phase difference of active voltage ports generated a uniform birdcage-like mode for the 3-channel labeling coil.

In Vivo Experiments

All procedures performed in studies involving human participants were in accordance with the ethical standards of the University of Pennsylvania and the National Institutes of Health. All equipment and pulse sequences were approved by the University of Pennsylvania Internal Review Board prior to *in vivo* use. Coil approval was based on the ASTM International standard (International 2011). Informed written consent was obtained from all individual participants prior to their inclusion in this study. Data were acquired from five

healthy volunteers (3 F, median age 26 ± 3.3 years) on a Siemens Magnetom 7 T scanner (Siemens Healthcare, Erlangen, Germany).

The labeling coils were centered over the hinge of the jaw bilaterally and at the back of the neck, while the head was centered in the head coil volume. Following localizer acquisitions, a 10-slice axial 2D FLASH data set was acquired with the labeling coil to identify the optimal labeling plane as having the carotid and vertebral arteries running parallel to the B_0 field. The FLASH acquisition parameters were: TR/TE/flip angle 6.4 ms/2.8 ms/25° acquired with a 30-cm field-of-view (FOV), a 5-mm slice thickness and a 256 × 256 acquisition matrix.

To demonstrate the elimination of MT effects from active decoupling of the head coil during labeling, image data were acquired using single-slice echo-planar imaging (EPI) with a 4500-ms TR, 18-ms TE, and a 45° flip angle with varying labeling conditions. The EPI slice thickness was 3-mm, the FOV was 22-cm, and acquisition matrix was 128 ×128. Ten images were acquired (five pairs with alternating RF power on and off) with labeling gradient values of: 0.25, 0.50, 0.75, 1.00, 1.25, 1.50, 2.00, 2.50 and 3.00 mT/m. In order to eliminate any perfusion confounds from the experiment, the resonant frequency of the RF was tuned to a plane distal to the imaging slice. Off-resonance pulses were applied during a 2000-ms control RF train (consisting of 50-ms square pulses with a 99% duty cycle and 40-Volt reference voltage) at a frequency offset corresponding to 10-cm superior to the imaging plane, followed by 100 ms of post-control delay. The resulting images from the 9 labeling gradient data sets were aligned using affine registration using SPM12 (Wellcome Trust Centre for Neuroimaging, UCL, London, UK) prior to calculating the magnetization transfer ratio (MTR) (Dousset et al., 1992). A large region-of-interest (ROI) was drawn over the slice, excluding areas of large susceptibility artifact and cerebrospinal fluid (CSF) for analysis (Figure 5a).

The B_1 profile was measured using the dual-TR gradient-recalled echo (GRE) actual flip-angle imaging (AFI) method (Yarnykh 2007). Prior to the B_1-mapping acquisition, standard vendor-supplied B_0 phasemap high order shimming was performed on the brain volume using the head coil Tx/Rx only, thus ensuring an accurate representation of the true B_0 field at the level of the labeling plane during subsequent CASL experiments. The acquisition parameters for the 2D AFI sequence were as follows: 80-ms long TR (TRl), 20-ms short TR (TRs), 10-ms TE, 30° flip angle, 16 slices centered around the chosen labeling plane, a 2D acquisition matrix of 128 × 128, a 2-mm slice thickness, and a 25.6-cm FOV. B_1 maps were generated from the ratio of the images collected with the short and long TR according to Equation 6 given by Yarnykh (Yarnykh 2007). Regions of interest were drawn over the left and right internal carotid arteries (LICA and RICA) and the left and right vertebral arteries (LVA and RVA) from the short-TR image for each participant; labeling efficiency was estimated from each vessel based on simulations by Maccotta *et al.* (Maccotta et al., 1997), and using nominal mean blood flow velocities reported in MacDonald *et al.* (MacDonald and Frayne 2015).

B_0 mapping was also performed to determine the extent of off-resonance in the labeling plane. The same high-order shim parameters from the head coil that were used in the B_1-

mapping acquisition were applied for the B_0-mapping acquisition, thus ensuring worst-case scenario for the B_0 profile at labeling plane. A coronal 2D dual-echo GRE B_0-mapping sequence was acquired across the neck in each participant (Yeo et al., 2007). Sequence parameters for the B_0-mapping acquisition were as follows: 800-ms TR, 10-ms short echo time (TEs), 11.02-ms long echo time (TEl), 45° flip angle, 30 slices centered on the neck, a 25-cm FOV at 128 × 128, and a 5-mm slice thickness. Similar to the B_1-mapping procedure, regions of interest were drawn over the left and right internal carotid arteries and the left and right vertebral arteries from the short-TE image for each participant. The measured off-resonance was then incorporated into the labeling efficiency calculations for comparison.

Perfusion imaging experiments were performed using CASL acquisitions with 30 label/control pairs (60 alternating label and control images). The CASL labeling duration was initially set at 2000 ms (consisting of 50-ms square pulses with a 99% duty cycle and 40-Volt reference voltage), with a 1250-ms post-label delay. The labeling gradient was 2.50 mT/m, and no RF pulses were applied during control acquisitions. These settings yielded a SAR-minimum TR of 7300 ms.

CASL effects were measured using EPI acquired with a 220-cm FOV at 128 × 128, 16 slices at 3-mm slice thickness and a 25% slice gap, a TE of 18 ms with a GRAPPA factor of 3. Affine motion correction was performed using the ASL toolbox (Wang 2012, Wang et al., 2008) with SPM12, and ASL analysis was performed using MATLAB (The MathWorks, Natick, MA). For each subject, percent signal map time series was derived by pairwise control-label subtraction and dividing by the mean control image. The mean percent signal change map was derived from the time series of the percent signal maps using a two-step procedure; (i) a structural correlation based outlier rejection (SCORE) method which explicitly detects and discards outlier volumes iteratively (Dolui et al., 2015), followed by (ii) a voxel-wise robust Bayesian estimation approach (Yuanxi 1991). Slice timing correction was applied to the mean percent signal change map to account for differences in post-label delay. Conservative binary brain segmentation was performed on the mean images for each CASL data set in SPM12. A binary mask was created for gray matter (GM) by setting any voxels above the 95% threshold to 1; all others were set to 0. In order to evaluate the impact of the estimated labeling efficiency from each vessel in the labeling plane on the ΔM% maps, known vascular territory ROIs were generated for the left and right middle cerebral artery (MCA) territories and a combined ROI that encompasses the left and right posterior cerebral arteries (PCA, Figure 5) (Luh et al., 2013). These simulated vascular territory ROIs were drawn on the 2-mm MNI152 atlas and co-registered to the anatomical data for each participant. Mean and standard deviation were recorded for the GM masks for each individual.

Results

MT Experiments

Figure 4 shows the mean result of the MT experiment across 5 subjects, plotted with standard deviation. As shown, increasing the labeling gradient above 2 mT/m demonstrates a MTR of 0.0% (standard deviation of ± 0.2%). The slight negative trend of the MTR at higher gradient strengths can be attributed to random noise fluctuations, and are within one

standard deviation of zero mean. This result suggests our labeling gradient of 2.5 mT/m for the CASL experiments is sufficient to eliminate MT, thus allowing for control schemes that do not require MT-matching RF.

Simulated B_1 Mapping and AFI B_1 Mapping

The results of the xFDTD are shown in Figure 3. The spatial phase distribution of the simulated B_1-field is consistent with other 7 T transceiver coils (Van de Moortele et al., 2005). The results of the AFI B_1-mapping acquisitions are shown in Figure 5 for all 5 subjects. As demonstrated, the B_1 profile from the three-coil system is in agreement with the results of the xFDTD simulation. The discrepancies between the *in vivo* results and the simulation can be attributed to variations in the placement of the labeling coils on the neck brace, susceptibility effects in the throat and mouth areas, and physical differences between the simulation model and subjects. The mean B_1 achieved across the group for the LICA and RICA was 2.95 μT (standard error, SE ± 0.08 μT) and 2.76 μT (SE ± 0.08 μT), and 2.71 μT (SE ± 0.15 μT) and 0.75 μT (SE ± 0.14 μT) for the LVA and RVA, respectively. Without taking into account off-resonance in the labeling plane, and based solely on the positions of the vessels of interest in the B_1 maps, the group mean estimated labeling efficiency in the LICA and RICA was 88.6% (standard error, SE ± 8.5%) and 85.9% (SE ± 10.1%), and 96.0% (SE ± 13.5%) and 54.3% (SE ± 19.9%) for the LVA and RVA, respectively. Due to the mixing of vertebral blood in the basilar artery distal to the Circle of Willis, the estimated labeling efficiency delivered to the bilateral PCA territories was assumed to be 78.8% (SE ± 16.1%), based on the slightly higher expected bulk flow volume in the left vertebral artery.

B_0 Mapping

The results of the B_0 mapping experiments are shown for all 5 subjects in the bottom row in Figure 5. The group mean estimated off-resonance in the LICA and RICA was 818 Hz (SE ± 271 Hz) and 793 Hz (SE ± 215 Hz), and 705 Hz (SE ± 289 Hz) and 403 Hz (SE ± 665 Hz) for the LVA and RVA, respectively. The large standard errors of the vertebral arteries are reflective of the limited number of voxels used in each measurement. When including the off-resonance measurements in the labeling efficiency estimations, the group mean estimated labeling efficiency in the left and right internal carotid arteries was 48.0% (SE ± 12.1%) and 34.7% (SE ± 8.8%), and 55.3% (SE ± 11.9%) and 25.4% (SE ± 25.9%) for the left and right vertebral arteries, respectively. Similar to the uncorrected labeling efficiency calculation, the expected bilateral PCA delivered efficiency was 43.0% (SE ± 17.7%). As shown in Figure 7, off-resonance has a significant negative impact on labeling efficiency.

CASL Cerebral Blood Flow Experiments

Sample perfusion-weighted ΔM% results from all five healthy volunteers are shown in Figure 6. The outlier detection method rejected 3/59, 6/59, 8/59, 15/59, and 5/59 interpolated label-control pairs for subjects 1–5, respectively (Dolui et al., 2015). In all subjects, the percent difference maps did not correspond to the uncorrected labeling efficiency measurements. Rather, the percent change maps were more reflective of the off-resonance corrected estimated labeling efficiency across the internal carotid arteries and the vertebral arteries (Figures 3–5), including the noted left-right hemispheric asymmetries in the ΔM% maps in Subjects 4 and 5. The acquired spatial resolution was 1.5 × 1.5 × 3.0

mm^3, which is >10 times smaller than typical ASL voxels acquired at 3 T (e.g., 3.75 × 3.75 mm^2 in-plane with 5.0 (Dai et al., 2008) or 6.0 (Chen et al., 2011) mm slice thickness). The average gray matter (GM) percent signal change for all subjects was 1.01% (SE ± 0.05%) for the left MCA territory, 0.98% (SE ± 0.05%) for the left MCA territory, and 0.99% (SE ± 0.10%) for the bilateral MCA territory. These ΔM% values correspond with the lower-than-expected estimated labeling efficiency for CASL.

Discussion

This study was designed to assess the feasibility of using an actively decoupled dual coil system to perform CASL MRI at 7 T. Active decoupling of the head coil during labeling was shown to successfully eliminate MT in the brain from labeling reducing the total label/control SAR deposition by 50% as compared to the use of an active control labeling approach. Despite this, TR was still SAR limited at 7.3s with a 2 sec labeling duration, which remains below the labeling duration that would be required to maximize ASL effects at 7 T, even though RF deposition during imaging was minimized by using EPI without background suppression. Based on the blood T_1 of 2066 ms at 7 T (Dobre et al., 2007), a labeling duration of over 5000 ms would be required for to achieve the assumed steady-state condition for maximal labeling of brain water (Lu et al., 2010), and would result in a SAR-minimum TR of approximately 45 sec. Future refinements in SAR modeling and monitoring for 7 T studies may allow the SAR-minimum TR to be reduced, which would greatly benefit the practical feasibility of 7 T ASL using dual coil CASL. As mentioned in the introduction, previously published 7 T pCASL research either used very short labeling durations (Ghariq et al., 2012) or data were collected on an antiquated 7 T system that may have used more liberal SAR calculation limits (Luh et al., 2013). Thus, a consistent implementation of 7 T pCASL with a sufficient labeling duration remains elusive (Lu et al., 2010).

During development of this system, the performance of the active detuning was confirmed both in a phantom and *in vivo*. To accomplish this, the head and labeling coils were configured as transceivers to evaluate their performance and possible interactions between the coils during RF transmission with the labeling coil via TTL RF switch control. As shown in Figure 2, the RF switch was not configured to provide detuning to the labeling coils during RF excitation with the head coil. This is not a limitation of the experimental design, given that the SAR-minimum TR was >7000 ms, and any unexpected coupled excitation of arterial blood during RF application in the head coil will have fully recovered prior to the next label/control acquisition. Due to the configuration of the three labeling coils, the resulting shape of the B_1-field (Figure 3c) has the potential for reduced B_1 amplitude in the right vertebral artery. This is demonstrated in both our estimated labeling efficiencies and the CASL ΔM% maps, particularly in Subject 4. Coil placements should be considered in future coil designs to reduce this limitation.

One limitation of the experimental design is that the actual blood flow velocities in the internal carotid arteries and vertebral arteries were not measured for each subject (Aslan et al., 2010), and instead literature values used for the efficiency calculations (MacDonald and Frayne 2015). Similarly, the vascular territories were derived using an *a priori* atlas-based approach, rather than performing any advanced vessel-encoded ASL strategies (Wong 2007).

As reported, the percent signal change observed in GM is well below the expected ΔM% of approximately 2.4% (Figure 1a). As demonstrated in our results accounting for the B_1 profile and B_0 inhomogeneity in the labeling plane, our labeling efficiency is well below the expected 85% for CASL. The heterogeneities observed in the B_1 field measured in the regions of interest shown in Figures 5 and 7 do not account for the observed reduction in labeling efficiency apparent in the CASL data in Figure 6. The large off-resonance measured in the labeling plane is clearly the most significant culprit for the reduction in labeling efficiency, as explained by the simulation in Figure 1b. One consequence of the circuit design of the coil system presented in Figure 2c is that the RF power from the vendor-supplied RF amplifier is exclusively routed to either the head coil or the labeling coil by the TTL switch. Thus, simultaneous transmission, and there-by simultaneous high-order shimming of the volumes in both coils is not available. Given the detrimental impact of B_0 inhomogeneity in the labeling plane demonstrated here, future work should focus on system designs that allow for simultaneous shimming of the labeling and head coil volumes, or advanced dynamic shimming approaches that allow for reduced off-resonance in the labeling plane.

The experimental results also reveal the challenges of generating a uniform B_1 field in the presence of multi-coil potential phase cancellation. In several subjects, B_1-mapping was able to identify the source of failure of the CASL labeling efficiency, due to poor B_1-profile. As shown in Figure 3a, this also highlights the second major limitation discussed previously: labeling efficiency is still heavily dependent on B_1 homogeneity across the vessels of interest. One method for improving the consistency of this B_1 profile is the addition of parallel transmit (Adriany et al., 2005), however an accurate SAR model is paramount for such an endeavor *in vivo* (Eichfelder and Gebhardt 2011). These findings illustrate the complexity of achieving efficient CASL at 7 T, and the necessity for labeling coils to include receive capabilities.

Based on the measured B_0-corrected labeling efficiency, the achieved GM ΔM% is comparable to the level expected from PASL at 7 T (Zuo et al., 2013), though this assumes that PASL inversion efficiency is not also compromised by B_1 inhomogeneity in the labeling slab, and that the bolus length is not limited by coil coverage in the superior-inferior direction. Further improvements to the labeling coil designs could possibly yield GM ΔM% that is much higher than can be achieved with PASL. Alternatively, a coil system with longer superior-inferior coverage might be used in future work using PASL, thereby generating a larger inversion bolus than is available currently.

Conclusion

Using an actively decoupled dual transceiver system, it was possible to decouple neck labeling and brain imaging coils such that magnetization transfer effects of labeling were eliminated and CASL perfusion MRI could be performed without the need for control labeling. Despite this, SAR limitations on labeling B_1 precluded achieving the full benefit of continuous ASL at 7 T within acceptable repetition times, and the resulting labeling efficiency ultimately remained comparable to pulsed labeling. Furthermore, B_0 inhomogeneities at the labeling location contributes to further reductions in labeling

efficiency that are variable across subjects and arteries. Thus, while ASL effects are increased at 7 T versus 3 T and can be potentially translated to improved sensitivity and resolution, further technical developments will be required to realize the potential benefits of 7 T ASL for basic and clinical neuroscience applications.

Acknowledgments

Financial Acknowledgements and Sponsorship:

NIH P41-EB015893, NIH T32-EB000814, NRF-2015M3C7A1031969

This project was a collaboration between the Neuroscience Research Institute at Gachon University and researchers at the University of Pennsylvania. This research was supported by the National Institutes of Health (NIH P41-EB015893) and by the Brain Research Program through the National Research Foundation of Korea (NRF) funded by the Ministry of Science, ICT & Future Planning (NRF-2015M3C7A1031969).

All 7 T MR image data were collected at the Center for Magnetic Resonance and Optical Imaging at the University of Pennsylvania. Dr. R.B. Stafford is now located at the University of Calgary; M.K. Woo is now located at the University of Minnesota; Dr. S.H. Oh is now located at the Imaging Institute at the Cleveland Clinic; Dr. Z.H. Cho is now located at Seoul National University; and Dr. J. Lee is now located at the Laboratory for Imaging Science and Technology (LIST) at Seoul National University.

The authors would like to thank Dr. Tom Connick for all of his assistance developing the final labeling coil design and configuration, as well as his help getting the entire system approved by IRB for these experiments. Drs. Hari Harihan and Mark Elliott were instrumental in helping implement the B_1- and B_0- mapping sequences. Lastly, the authors would like to extend their deep gratitude to all of their participants.

Important Abbreviations

ASL	Arterial Spin Labeling
CASL	Continuous ASL
pCASL	pseudo-CASL
PASL	Pulsed ASL
MT	Magnetization Transfer
Tx/Rx	Transmit/Receive
TTL	Transistor-Transistor Logic
AFI	Actual Flip-angle Imaging
GM	Gray Matter
CSF	CerebroSpinal Fluid
UHF	Ultra-high field

References

Adriany G, Van de Moortele PF, Wiesinger F, Moeller S, Strupp JP, Andersen P, Snyder C, Zhang X, Chen W, Pruessmann KP, Boesiger P, Vaughan T, Ugurbil K. Transmit and receive transmission line arrays for 7 tesla parallel imaging. Magn Reson Med. 2005; 53:434–445. [PubMed: 15678527]

Alsop DC, Detre JA. Reduced transit-time sensitivity in noninvasive magnetic resonance imaging of human cerebral blood flow. J Cerebr Blood F Met. 1996; 16:1236–1249.

Alsop DC, Detre JA. Multisection cerebral blood flow mr imaging with continuous arterial spin labeling. Radiology. 1998; 208:410–416. [PubMed: 9680569]

Aslan S, Xu F, Wang PL, Uh J, Yezhuvath US, van Osch M, Lu H. Estimation of labeling efficiency in pseudocontinuous arterial spin labeling. Magn Reson Med. 2010; 63:765–771. [PubMed: 20187183]

Brown GG, Clark C, Liu TT. Measurement of cerebral perfusion with arterial spin labeling: Part 2. Applications. J Int Neuropsych Soc. 2007; 13:526–538.

Chen JJ, Rosas HD, Salat DH. Age-associated reductions in cerebral blood flow are independent from regional atrophy. Neuroimage. 2011; 55:468–478. [PubMed: 21167947]

Chen Y, Wang DJ, Detre JA. Test-retest reliability of arterial spin labeling with common labeling strategies. J Magn Reson Imaging. 2011; 33:940–949. [PubMed: 21448961]

Collins CM, Smith MB. Calculations of b(1) distribution, snr, and sar for a surface coil adjacent to an anatomically-accurate human body model. Magn Reson Med. 2001; 45:692–699. [PubMed: 11283998]

Dai W, Garcia D, de Bazelaire C, Alsop DC. Continuous flow-driven inversion for arterial spin labeling using pulsed radio frequency and gradient fields. Magn Reson Med. 2008; 60:1488–1497. [PubMed: 19025913]

Detre JA, Alsop DC. Perfusion magnetic resonance imaging with continuous arterial spin labeling: Methods and clinical applications in the central nervous system. Eur J Radiol. 1999; 30:115–124. [PubMed: 10401592]

Detre JA, Leigh JS, Williams DS, Koretsky AP. Perfusion imaging. Magn Reson Med. 1992; 23:37–45. [PubMed: 1734182]

Dixon WT, Du LN, Faul DD, Gado M, Rossnick S. Projection angiograms of blood labeled by adiabatic fast passage. Magn Reson Med. 1986; 3:454–462. [PubMed: 3724425]

Dobre MC, Ugurbil K, Marjanska M. Determination of blood longitudinal relaxation time (t1) at high magnetic field strengths. Magn Reson Imaging. 2007; 25:733–735. [PubMed: 17540286]

Dolui, S.; Wang, Z.; Wolk, DA.; Detre, JA. An outlier rejection algorithm for asl time series: Validation with adni control data. Proceedings 23rd Scientific Meeting, International Society for Magnetic Resonance in Medicine; 2015; p. 2356

Dousset V, Grossman RI, Ramer KN, Schnall MD, Young LH, Gonzalez-Scarano F, Lavi E, Cohen JA. Experimental allergic encephalomyelitis and multiple sclerosis: Lesion characterization with magnetization transfer imaging. Radiology. 1992; 182:483–491. [PubMed: 1732968]

Edelman RR, Siewert B, Darby DG, Thangaraj V, Nobre AC, Mesulam MM, Warach S. Qualitative mapping of cerebral blood flow and functional localization with echo-planar mr imaging and signal targeting with alternating radio frequency. Radiology. 1994; 192:513–520. [PubMed: 8029425]

Edelstein WA, Glover GH, Hardy CJ, Redington RW. The intrinsic signal-to-noise ratio in nmr imaging. Magn Reson Med. 1986; 3:604–618. [PubMed: 3747821]

Eichfelder G, Gebhardt M. Local specific absorption rate control for parallel transmission by virtual observation points. Magn Reson Med. 2011; 66:1468–1476. [PubMed: 21604294]

Frahm J, Haase A, Matthaei D. Rapid nmr imaging of dynamic processes using the flash technique. Magn Reson Med. 1986; 3:321–327. [PubMed: 3713496]

Franke C, van Dorsten FA, Olah L, Schwindt W, Hoehn M. Arterial spin tagging perfusion imaging of rat brain: Dependency on magnetic field strength. Magn Reson Imaging. 2000; 18:1109–1113. [PubMed: 11118765]

Gardener AG, Gowland PA, Francis ST. Implementation of quantitative perfusion imaging using pulsed arterial spin labeling at ultra-high field. Magn Reson Med. 2009; 61:874–882. [PubMed: 19189295]

Gardener AG, Jezzard P. Investigating white matter perfusion using optimal sampling strategy arterial spin labeling at 7 tesla. Magn Reson Med. 2015; 73:2243–2248. [PubMed: 24954898]

Ghariq E, Teeuwisse WM, Webb AG, van Osch MJ. Feasibility of pseudocontinuous arterial spin labeling at 7 t with whole-brain coverage. Magn Reson Mater Phy. 2012; 25:83–93.

Gonen O, Gruber S, Li BS, Mlynarik V, Moser E. Multivoxel 3d proton spectroscopy in the brain at 1.5 versus 3.0 t: Signal-to-noise ratio and resolution comparison. Am J Neuroradiol. 2001; 22:1727–1731. [PubMed: 11673168]

Govindarajan ST, Cohen-Adad J, Sormani MP, Fan AP, Louapre C, Mainero C. Reproducibility of t2 * mapping in the human cerebral cortex in vivo at 7 tesla mri. J Magn Reson Imaging. 2015; 42:290–296. [PubMed: 25407671]

Hall, E.; Wesolowski, R.; Gowland, P.; Francis, S. Improved detection and estimation of perfusion using high spatial resolution asl at 7t. Proceedings 17th Scientific Meeting, International Society for Magnetic Resonance in Medicine; 2009; p. 1529

Hetzer S, Mildner T, Driesel W, Weder M, Moller HE. Shielded dual-loop resonator for arterial spin labeling at the neck. J Magn Reson Imaging. 2009; 29:1414–1424. [PubMed: 19472417]

A. International. Standard test method for measurement of radio frequency induced heating on or near passive implants during magnetic resonance imaging. ASTM International; West Conshohocken, PA. 2011; p. 14

Jahng GH, Zhu XP, Matson GB, Weiner MW, Schuff N. Improved perfusion-weighted mri by a novel double inversion with proximal labeling of both tagged and control acquisitions. Magn Reson Med. 2003; 49:307–314. [PubMed: 12541251]

Jung Y, Wong EC, Liu TT. Multiphase pseudocontinuous arterial spin labeling (mp-pcasl) for robust quantification of cerebral blood flow. Magn Reson Med. 2010; 64:799–810. [PubMed: 20578056]

Kim SG. Quantification of relative cerebral blood flow change by flow-sensitive alternating inversion recovery (fair) technique: Application to functional mapping. Magn Reson Med. 1995; 34:293–301. [PubMed: 7500865]

Kwong KK, Chesler DA, Weisskoff RM, Donahue KM, Davis TL, Ostergaard L, Campbell TA, Rosen BR. Mr perfusion studies with t1-weighted echo planar imaging. Magn Reson Med. 1995; 34:878–887. [PubMed: 8598815]

Lu H, Leoni R, Silva AC, Stein EA, Yang Y. High-field continuous arterial spin labeling with long labeling duration: Reduced confounds from blood transit time and postlabeling delay. Magn Reson Med. 2010; 64:1557–1566. [PubMed: 20715292]

Luh WM, Talagala SL, Li TQ, Bandettini PA. Pseudo-continuous arterial spin labeling at 7 t for human brain: Estimation and correction for off-resonance effects using a prescan. Magn Reson Med. 2013; 69:402–410. [PubMed: 22488568]

Maccotta L, Detre JA, Alsop DC. The efficiency of adiabatic inversion for perfusion imaging by arterial spin labeling. NMR Biomed. 1997; 10:216–221. [PubMed: 9430351]

MacDonald ME, Frayne R. Phase contrast mr imaging measurements of blood flow in healthy human cerebral vessel segments. Physiol Meas. 2015; 36:1517–1527. [PubMed: 26020543]

Raitakari M, Nuutila P, Ruotsalainen U, Teras M, Eronen E, Laine H, Raitakari OT, Iida H, Knuuti MJ, Yki-Jarvinen H. Relationship between limb and muscle blood flow in man. J Physiol. 1996; 496(Pt 2):543–549. [PubMed: 8910236]

Rooney WD, Johnson G, Li X, Cohen ER, Kim SG, Ugurbil K, Springer CS Jr. Magnetic field and tissue dependencies of human brain longitudinal 1h2o relaxation in vivo. Magn Reson Med. 2007; 57:308–318. [PubMed: 17260370]

Schwarzbauer C, Morrissey SP, Haase A. Quantitative magnetic resonance imaging of perfusion using magnetic labeling of water proton spins within the detection slice. Magn Reson Med. 1996; 35:540–546. [PubMed: 8992204]

Silva AC, Zhang W, Williams DS, Koretsky AP. Multi-slice mri of rat brain perfusion during amphetamine stimulation using arterial spin labeling. Magn Reson Med. 1995; 33:209–214. [PubMed: 7707911]

Stafford, RB.; Woo, MK.; Kim, KN.; Oh, SH.; Kim, YB.; Cho, ZH.; Detre, JA.; Lee, J. Continuous asl at 7t using a dual coil system: Initial experience. Proceedings of the International Society for Magnetic Resonance in Medicine Scientific Workshop, Perfusion MRI: Standardization, Beyond CBF & Everyday Clinical Applications; 2012;

Talagala, S.; Li, T.; Merkle, H.; Wang, S.; Bodurka, J.; van Gelderen, P.; Duyn, J. Comparison of continuous arterial spin labeling perfusion mri at 7t and 3t. Proceedings 16th Scientific Meeting, International Society for Magnetic Resonance in Medicine; 2008; p. 1916

Talagala SL, Ye FQ, Ledden PJ, Chesnick S. Whole-brain 3d perfusion mri at 3.0 t using casl with a separate labeling coil. Magn Reson Med. 2004; 52:131–140. [PubMed: 15236376]

Teeuwisse WM, Webb AG, van Osch MJ. Arterial spin labeling at ultra-high field: All that glitters is not gold. Int J Imag Syst Tech. 2010; 20:62–70.

Trampel R, Mildner T, Goerke U, Schaefer A, Driesel W, Norris DG. Continuous arterial spin labeling using a local magnetic field gradient coil. Magn Reson Med. 2002; 48:543–546. [PubMed: 12210922]

Van de Moortele PF, Akgun C, Adriany G, Moeller S, Ritter J, Collins CM, Smith MB, Vaughan JT, Ugurbil K. B(1) destructive interferences and spatial phase patterns at 7 t with a head transceiver array coil. Magn Reson Med. 2005; 54:1503–1518. [PubMed: 16270333]

van Gelderen P, de Zwart JA, Duyn JH. Pittfalls of mri measurement of white matter perfusion based on arterial spin labeling. Magn Reson Med. 2008; 59:788–795. [PubMed: 18383289]

Vaughan JT, Garwood M, Collins CM, Liu W, DelaBarre L, Adriany G, Andersen P, Merkle H, Goebel R, Smith MB, Ugurbil K. 7t vs. 4t: Rf power, homogeneity, and signal-to-noise comparison in head images. Magn Reson Med. 2001; 46:24–30. [PubMed: 11443707]

Wang J, Alsop DC, Li L, Listerud J, Gonzalez-At JB, Schnall MD, Detre JA. Comparison of quantitative perfusion imaging using arterial spin labeling at 1.5 and 4.0 tesla. Magn Reson Med. 2002; 48:242–254. [PubMed: 12210932]

Wang J, Zhang Y, Wolf RL, Roc AC, Alsop DC, Detre JA. Amplitude-modulated continuous arterial spin-labeling 3.0-t perfusion mr imaging with a single coil: Feasibility study. Radiology. 2005; 235:218–228. [PubMed: 15716390]

Wang, S.; Merkle, H.; Talagala, L. Sar evaluation of 7.0 tesla perfusion imaging with arterial spin labeling coil. Proceedings 16th Scientific Meeting, International Society for Magnetic Resonance in Medicine; 2008; p. 1046

Wang Y, Moeller S, Li X, Vu AT, Krasileva K, Ugurbil K, Yacoub E, Wang DJ. Simultaneous multi-slice turbo-flash imaging with caipirinha for whole brain distortion-free pseudo-continuous arterial spin labeling at 3 and 7 t. Neuroimage. 2015; 113:279–288. [PubMed: 25837601]

Wang Z. Improving cerebral blood flow quantification for arterial spin labeled perfusion mri by removing residual motion artifacts and global signal fluctuations. Magn Reson Imaging. 2012; 30:1409–1415. [PubMed: 22789842]

Wang Z, Aguirre GK, Rao H, Wang J, Fernandez-Seara MA, Childress AR, Detre JA. Empirical optimization of asl data analysis using an asl data processing toolbox: Asltbx. Magn Reson Imaging. 2008; 26:261–269. [PubMed: 17826940]

Williams DS, Detre JA, Leigh JS, Koretsky AP. Magnetic resonance imaging of perfusion using spin inversion of arterial water. Proceedings of the National Academy of Sciences of the United States of America. 1992; 89:212–216. [PubMed: 1729691]

Wong EC. Vessel-encoded arterial spin-labeling using pseudocontinuous tagging. Magn Reson Med. 2007; 58:1086–1091. [PubMed: 17969084]

Wong EC, Buxton RB, Frank LR. Quantitative imaging of perfusion using a single subtraction (quipss and quipss ii). Magn Reson Med. 1998; 39:702–708. [PubMed: 9581600]

Woo, MK.; Lee, J.; Kim, KN.; HOh, S.; Kim, YB.; Cho, ZH. Development of a coil for arterial spin labeling at 7t. Proceedings of the International Society for Magnetic Resonance in Medicine Scientific Workshop, Perfusion MRI: Standardization, Beyond CBF & Everyday Clinical Applications; 2012;

Wu WC, Fernandez-Seara M, Detre JA, Wehrli FW, Wang J. A theoretical and experimental investigation of the tagging efficiency of pseudocontinuous arterial spin labeling. Magn Reson Med. 2007; 58:1020–1027. [PubMed: 17969096]

Yarnykh VL. Actual flip-angle imaging in the pulsed steady state: A method for rapid three-dimensional mapping of the transmitted radiofrequency field. Magn Reson Med. 2007; 57:192–200. [PubMed: 17191242]

Yeo DT, Chenevert TL, Fessler JA, Kim B. Zero and first-order phase shift correction for field map estimation with dual-echo gre using bipolar gradients. Magn Reson Imaging. 2007; 25:1263–1271. [PubMed: 17442524]

Yuanxi Y. Robust bayesian estimation. B Geod. 1991; 65:145–150.

Zaharchuk G, Ledden PJ, Kwong KK, Reese TG, Rosen BR, Wald LL. Multislice perfusion and perfusion territory imaging in humans with separate label and image coils. Magn Reson Med. 1999; 41:1093–1098. [PubMed: 10371440]

Zuo Z, Wang R, Zhuo Y, Xue R, St Lawrence KS, Wang DJ. Turbo-flash based arterial spin labeled perfusion mri at 7 t. PloS one. 2013; 8:e66612. [PubMed: 23818950]

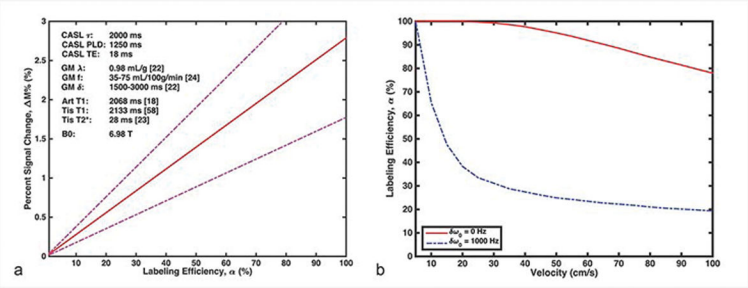

Figure 1.

a) Simulated percent signal change in gray matter (GM) as a function of B_0, assuming at an echo time (TE) of 18 ms, based on the simulations by Wang *et al.* (Wang et al., 2002). As shown in the diagram, with CASL labeling efficiency of 85%, the expected ΔM% at 7 T is around 2.4% for an expected blood flow of 55 mL/100 g/min (Chen et al., 2011). Other parameters for the simulation include arterial blood T_1 of 2068 ms (Dobre et al., 2007), a tissue T_2^* of 28 ms at 7 T (Govindarajan et al., 2015), and tissue T_1 of 2133 ms (Rooney et al., 2007). b) Simulation showing the impact of 1 kHz of off-resonance in the labeling plane based on simulations by Maccotta *et al.* (Maccotta et al., 1997).

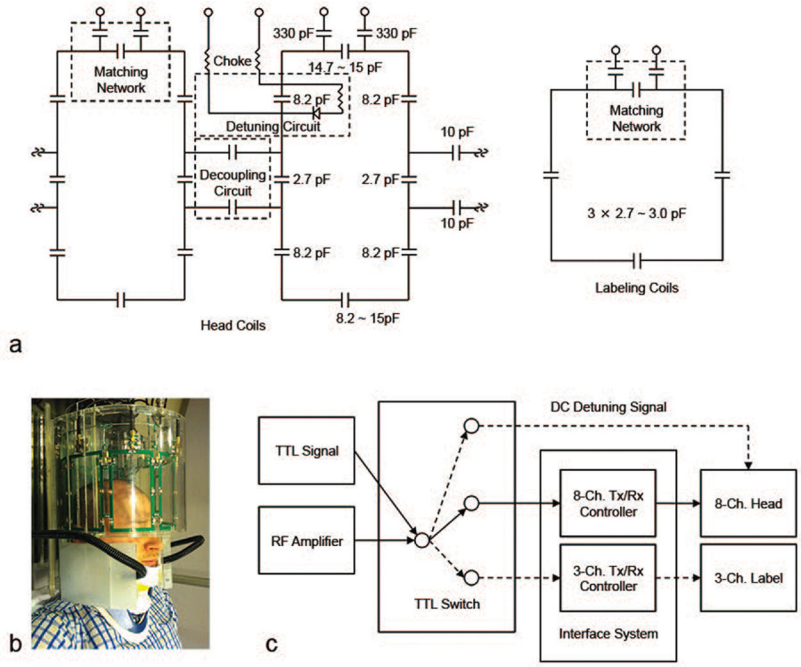

Figure 2.

Circuit diagram of the dual-coil 7 T ASL coil system. Diagram (a) represents a lumped-element equivalent circuit diagram of the head coil elements and with the active detuning circuitry indicated by the PIN diode. A circuit diagram for one of the labeling coil elements is shown on the right. The elliptical acrylic shell of the head coil is shown in image (b), along with the labeling coil. Diagram (c) is a schematic of the RF power routing and direct current (DC) detuning signal controlled by the TTL switch. When RF power is routed to the labeling coil, the DC detuning signal is sent to the head coil for decoupling.

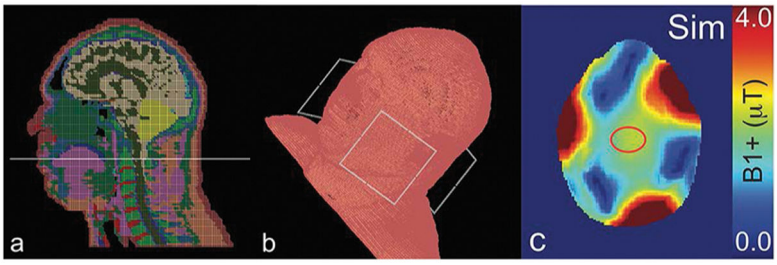

Figure 3.

Diagram of the B1-mapping. Images (a) and (b) represent screenshots from the xFDTD simulation for the labeling coil. The line in (a) indicates the chosen labeling plane for the simulation shown in (c). The red ROI in image (c) represents the calibration point to achieve a 90° tip with 3-ms rectangular pulse. The unit scale for image (c) is given in μT.

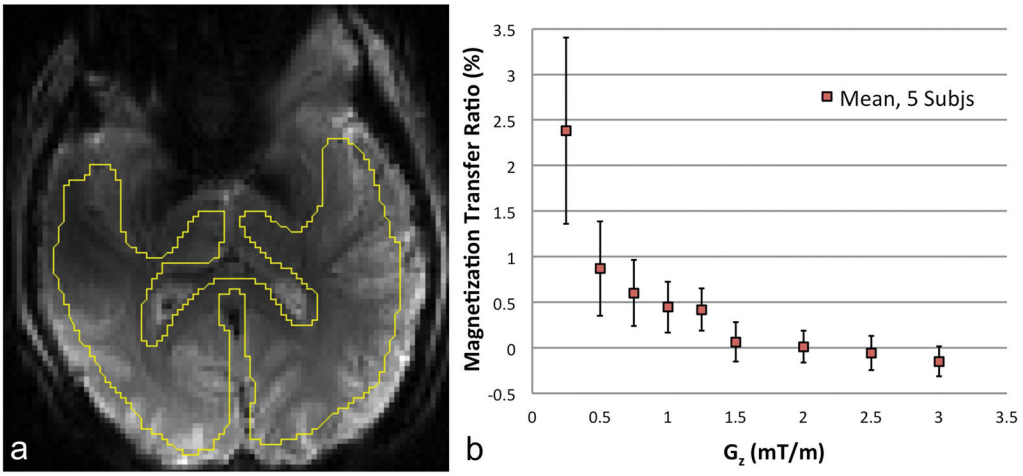

Figure 4.

Magnetization transfer (MT) experiment results obtained from five label/control pairs for 9 different labeling gradient values. RF power was not applied during labeling, only during control. Image (a) represents a sample single-slice EPI image from one of the five healthy volunteers. The ROI was drawn to exclude areas of high susceptibility distortion and CSF. Similar ROIs were drawn for all five subjects. The plot in (b) shows the mean magnetization transfer ratio (MTR) vs. labeling gradient strength in mT/m, plotted with standard deviation.

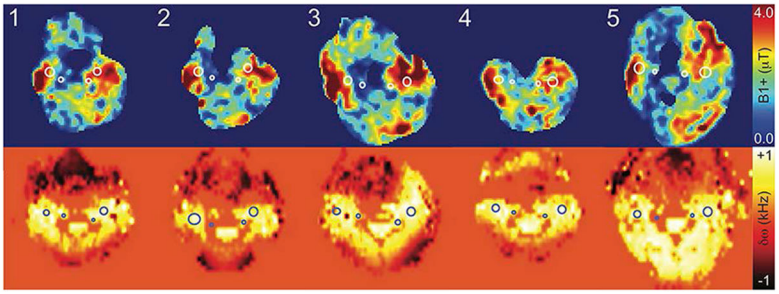

Figure 5.

Top) Results from the AFI experiment from the five participants (from left to right). The unit scale for these images is given in μT. The desired flip angle for AFI mapping was 30°, with a 3-ms pulse and a reference voltage of 200 V. The red ROIs in the top row and the blue ROIs in the bottom row indicate the positions of the left and right internal carotid arteries and left and right vertebral arteries, as determined from the corresponding anatomical references. Bottom) results of the B_0-mapping experiment from each of the participants. The unit scale for the B_0 maps are kHz.

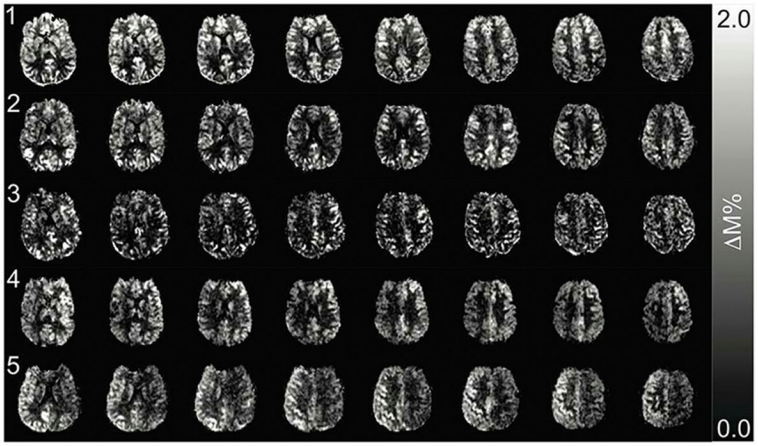

Figure 6.

Percent signal change maps from all five healthy volunteers (Subject 1 to 5 from top to bottom). These CASL data sets were acquired with 2000 ms of labeling, followed by 1250 ms of post-label delay using 30 label-control pairs.

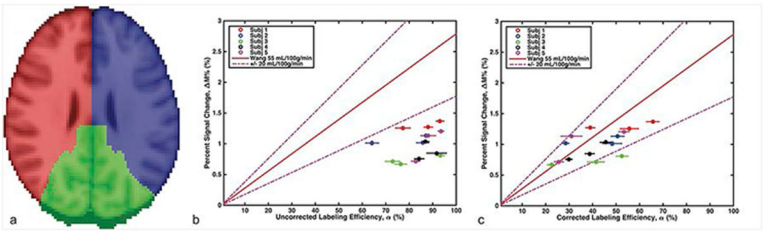

Figure 7.

a) Known cerebral perfusion vascular territory maps overlaid on the 2-mm MNI152 atlas. b) Vascular territory ΔM% measurements from all 5 participants, plotted vs. estimated labeling efficiency calculated without correction for B_0-inhomogeneity in the labeling plane. The estimated labeling efficiency values are well below the expected ΔM% values within physiologically relevant perfusion of 55 ± 20 mL/100 g/min indicated in red. c) The corresponding plot from b) with B_0-inhomogeneity corrected labeling efficiency estimates. These plots demonstrate that B_0-inhomogeneity is the main culprit in reduced labeling efficiency in our measurements.